Measurement and Evaluation of Display Scattering

Michael E. Becker

Display-Metrology & Systems - D 76135 Karlsruhe - Germany

www.display-metrology.com

Abstract

A novel approach is introduced for simple and effective measurement and evaluation of light scattering in general and its application to electronic displays is described. The method is based on the measurement of the lateral distribution of reflected luminance with an imaging detector. After numerical transformation of the measured luminance distribution we obtain the characteristics of the BRDF of the sample with high directional resolution within a limited range of inclination angles centered about the specular direction. The method is easy to implement and to carry out. Due to the absence of moving parts it exhibits only little sensitivity with respect to variations of the geometry parameters and is thus very robust. This paper summarizes the basics of the approach, establishes the relation to conventional BRDF-measuring methods, it introduces an implementation and presents some typical results for LCD-monitors.

Keywords

Display reflectance, glare, scattering, BRDF, PSF, ergonomic performance evaluation

1 Introduction

Since the first proposals to apply the method of the *bidirectional reflectance distribution function* (BRDF) to characterization of light scattering from visual displays [1, 2], only a limited number of BRDF-results obtained from commercial displays (e. g. LCD-monitors) have been published. Measurement and evaluation of BRDF-data still requires either a *mechanical system* for motorized scanning of the range of viewing-directions (or source-directions alternatively) or a *conoscopic system* that projects a collimated beam of light through its front-lens on the sample while catching all rays reflected from the spot of measurement. Besides the substantial investments for such instrumentation, an intrinsic weakness of the method is the fact that BRDFs obtained with different systems can only be compared in a qualitative way up to now. That means that, for example, the shape of the bell-shaped haze curve can be compared to those from other samples measured with the same apparatus, but evaluation of comparable numerical characteristics is still hardly possible, since theses characteristics (e. g. height of the specular peak on top of the haze-hill) are subject to substantial changes with the source-receiver signature of the respective systems [1, 3]. Moreover, numerical deconvolution to standardized source-receiver signatures as required for a comparison of the results on a common basis however becomes easier and more significant with increasing resolution of the results.

While high-resolution BRDF measurement and evaluation provides useful details about the directional reflectance of electronic display devices (e.g. height of specular peak on top of the haze-hill, directionality, diffraction and interference effects, etc.) the ergonomic rating of displays only requires the knowledge of a special subset: i.e., the specular reflectance factors for two sizes of source-aperture (e.g. 1° and 15° according to ISO 13406-2) and specific angles of incidence for calculation of the reflected luminance (causing *veiling glare*) under specified illumination conditions (diffuse and directional).

Measurement of the specular reflectance factor of electronic displays with a variable-aperture lightsource was introduced by Kubota in 1994 [4] and related to the concept of the BRDF in 2002 [5]. In this method a limitation arises from the fact that diffuse sources (based e.g. on integrating spheres) are used which

are supposed to provide a uniform luminance distribution across the exit port. At the same time however, a large amount of the light flux is wasted into directions which do not contribute to the measurement and thus, the fraction of flux illuminating the spot of measurement can be quite low and noise problems may arise in the detector for small source apertures. In addition to the decreasing signal to noise ratio also the alignment of the receiver system with respect to the specular direction becomes more difficult and even small deviations may cause large errors in the specular reflectance [6].

In order to provide the specular reflectance data over the required range with sufficient accuracy and robustness in combination with the detailed characteristics of high-resolution BRDF-data without mechanical scanning we introduce the following measurement approach:

- application of an imaging photometer instead of a spot-photometer,

- high-intensity small area source instead of a variable aperture source with integrating spheres,

- numerical data-processing to obtain the BRDF,

- numerical integration over receiver aperture to obtain the specular reflectance factors r_{S1} and r_{S15} (ISO-13406-2).

2 The point-spread-function

Figure 1: Luminance distribution obtained by reflection of a point-source in an LCD-monitor (point-spread-function, PSF).

Michael E. Becker

A simple arrangement is often used for demonstration of the basic features of the BRDF: the reflections of a sufficiently small source (point-source) in a display screen. This pattern of reflected light is deceptive because it looks very much like the BRDF of the sample with the haze component fading out with increasing distance from the specular peak. A second closer look however may suggest that this pattern cannot be the BRDF of the sample, because each spot on the sample surface is illuminated from a special direction and it reflects into another specific direction. The basic idea of the approach proposed here is to sample the reflected luminance from each spot on the sample, P(x, y) and to transform the reflectance values adequately to obtain the BRDF characteristics.

In order to derive a procedure for the transformation between a measured PSF and the BRDF we first introduce the geometry of the PSF measuring setup as shown in figure 2.
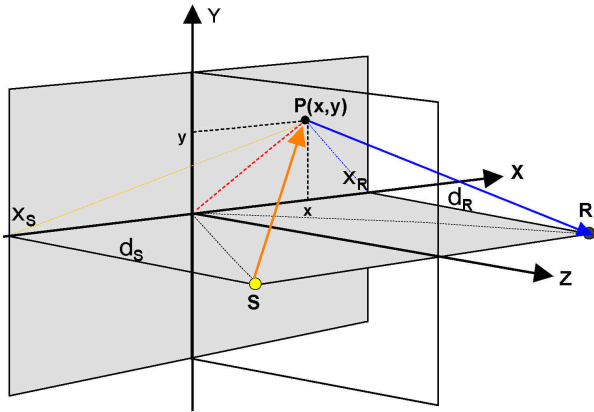

Figure 2: Setup for measurement of the PSF with isotropic lightsource S, imaging photometer (receiver) R and the device under test, DUT, located in the xy-plane The optical axis of the receiver goes through the origin of the xy-coordinate system.

2.1 PSF Geometry

For each area element dA(x, y) in the xy-plane and with the x and z-coordinates of light-source and receiver position, x_S, x_R, d_S, d_R, we obtain the *direction of light incidence* (from S to P) and the *direction of light reflected into the receiver* (from P to R) as follows (both vectors are not normalized):

$$\overrightarrow{SP} = \begin{bmatrix} x - x_S \\ y \\ -d_S \end{bmatrix}, \tag{1}$$

$$\overrightarrow{PR} = \begin{bmatrix} x_R - x \\ -y \\ d_R \end{bmatrix}. \tag{2}$$

In the symmetric case, $d_R = d_S$ and $\theta_R = \theta_S$, and for the spots P restricted to the x-axis, only the angles of inclination change at a constant azimuth ϕ (in-plane PSF).

3 Measurement of the BRDF

In order to derive the computation of the BRDF from the PSF we first have a closer look at the conventional measurement of the BRDF. In the arrangement for measuring the BRDF of a surface, an area element dA is illuminated from one direction, (θ_S, ϕ_S), and the reflected luminance is measured as a function of the direction of the received beam, (θ_R, ϕ_R), as shown in fig. 3 for a polar coordinate system centered about the surface-normal of the sample in location P.
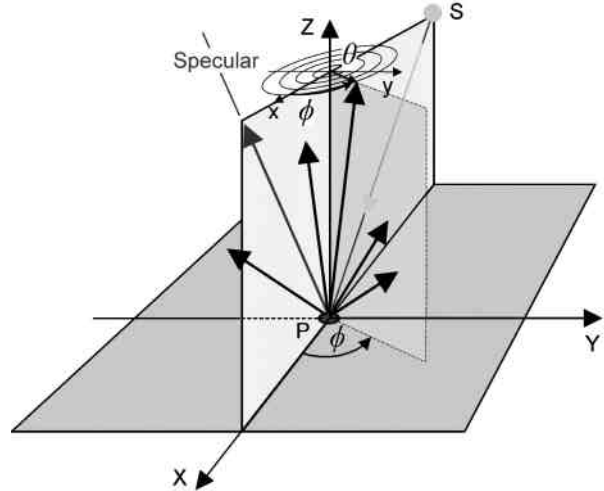

Figure 3: Polar coordinate system xy centered about the sample normal (z-axis) for specification of light-beams reflected in P with inclination θ and azimuth ϕ. Polar coordinate system x*y* shown displaced along the z-axis for clarity.

A typical BRDF of an LCD-screen measured with a conoscopic system according to fig. 3 is shown in fig. 4 in a polar coordinate system centered about the surface normal. The haze is centered about the specular direction ($\theta_R = \theta_S$, $\phi_R = \phi_R + 180°$), decreasing with increasing angular distance from specular. The right diagram shows the cross-section through the 2-dim. BRDF, the in-plane BRDF (IP-BRDF) as a function of the angle of receiver inclination, θ_R.
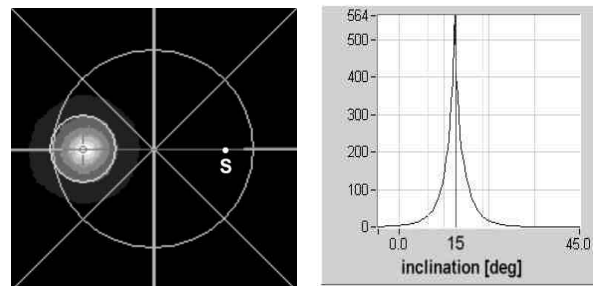

Figure 4: 2D-BRDF of an LCD-screen (left), $\theta_S = 15°$, source-location S, in-plane-BRDF (right diagram, cross-section at $\phi = 180°$). Conoscopic measmnt., system-signature FWHM ≈ 1°.

Alternatively, the beams reflected in P can be specified by two polar angles, θ^* and ϕ^* in an inclined coordinate system that is centered about the specular beam (see fig. 5). Here, both the x* and z*-axis of the inclined coordinate system lie in the xz-plane and the y*-axis remains parallel to the xy-plane.

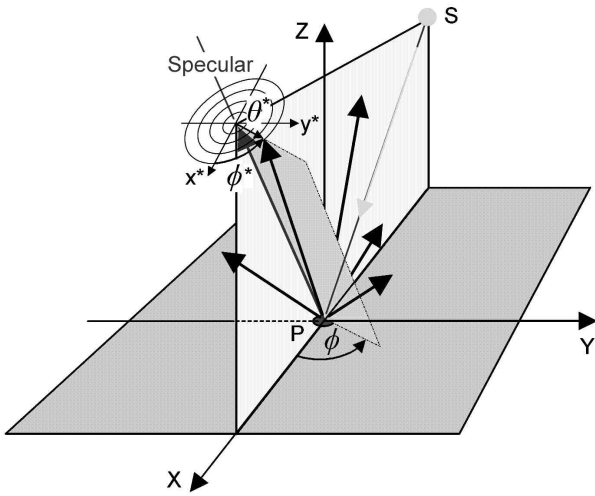**Figure 5:** Inclined polar coordinate system x*y*z* centered about the specular beam for specification of light-beams reflected in P by the polar angles θ^*_R, ϕ^*_R. Polar coordinate system x*y* shown displaced along the z*-axis for clarity.

The coordinates in the inclined system, x^*, y^* and z^* are related to the coordinates of the normal system, x, y and z, by:

$$\begin{bmatrix} x^* \\ y^* \\ z^* \end{bmatrix} = \begin{bmatrix} \cos\theta_R & 0 & -\sin\theta_R \\ 0 & 1 & 0 \\ \sin\theta_R & 0 & \cos\theta_R \end{bmatrix} \cdot \begin{bmatrix} x \\ y \\ z \end{bmatrix} \qquad (3)$$

4   From the PSF to the BRDF

The setup for the measurement of the PSF is sketched in fig. 2: an isotropic light-source S and an imaging photometer (receiver) R, are placed within a plane perpendicular to the device under test (DUT) in a specular configuration, $\theta_S = \theta_R$. The distance of source and receiver from the DUT has to be adjusted to obtain the required aperture angle of the receiver and subtense angle of the source. The combination of these dimensions gives the maximum deviation from the central ray,

$$\delta = atan((r_S + r_R) / (d_S/\cos\theta_S + d_R/\cos\theta_R)) \qquad (4)$$

with the radius of source and receiver aperture, r_S and r_R, respectively. Both apertures thus define the limit of the angular resolution of system which should be small enough to approximate the delta-impulse function as close as possible.

Experimental evaluation of the source-receiver signature, σ, is carried out either in the unfolded arrangement, or with a non-scattering front-surface mirror, taking for example, the FWHM as a characteristic value for the width (see fig. 7). Even though the aperture of the receiver is quite small (4mm) the receiver is focused on the light source in order to increase the angular resolution.

The distribution of luminance reflected from the area elements dA(x, y) on the DUT is measured with the imaging photometer R and the data is evaluated to obtain the BRDF as:

$$BRDF(\theta^*(x, y), \phi^*(x, y)) = dL(x, y) / dE(x, y). \qquad (5)$$
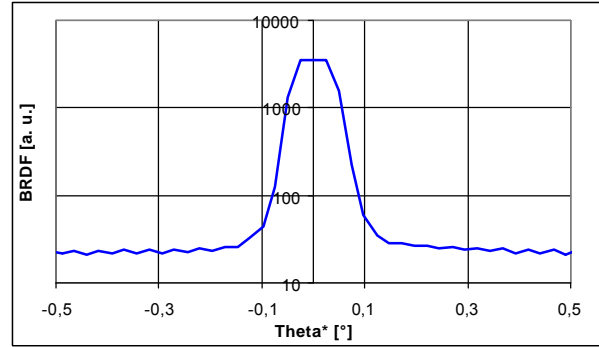

Figure 6: IP-BRDF from the PSF of the light source measured via a mirror (a.u. means *arbitrary units*). This function represents the source-receiver signature of the system with a FWHM of $\pm 0.05°$.

This definition takes into account that for each spot on the sample the direction of light incidence and the direction of light reflected into the receiver is different and thus the specular beam, PS*, is chosen as the reference direction at each location, P(x, y).

4.1   Transformation PSF to BRDF

For each pixel of the imaging photometer, $P_R(x', y')$, the location of the corresponding spot on the DUT, P(x, y), is computed and then, for each spot on the DUT the direction of light incidence and the direction of the beam reflected into the photometer, θ^* and ϕ^* is evaluated. Here, θ^* is the angle between the received beam, PR and the specular beam at the same location, PS*. The azimuth ϕ^* is given by the intersection of the plane containing both the reflected and the specular beam with the x*y*-plane as shown in fig 7. This choice is in strict analogy to the geometrical situation when measuring the BRDF according to the setup of fig. 5.
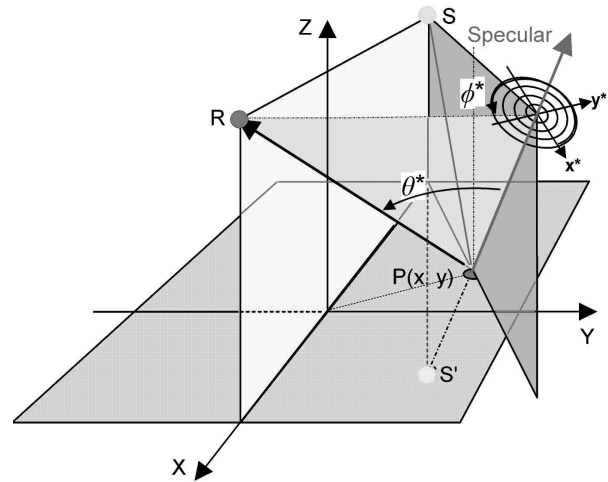

Figure 7: Inclined polar coordinate system x*y* centered about the specular beam (PS*) for specification of light-beams reflected from P into the receiver, R, by inclination θ^* and azimuth ϕ^*. Polar coordinate system x*y* shown displaced along the specular direction, PS*, for clarity.

Plotting both angles θ* and ϕ* (see appendix for derivation) for each column of pixels of the photometer in a polar coordinate system we obtain the lines shown in fig. 8. It is obvious that both columns and rows are transformed into curved lines that remain basically vertical and horizontal. A consequence of this transformation is (contrary to the second closer look as mentioned above) that we indeed see a slightly deformed BRDF when looking at the PSF from the direction of the specular beam.
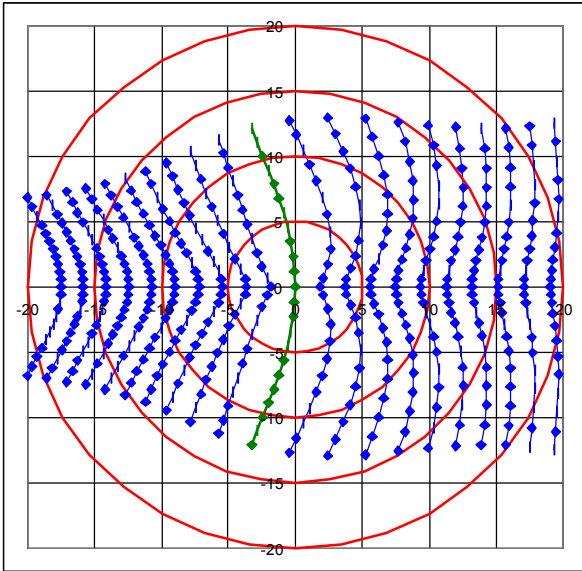

Figure 8: Loci of the pixels of the regular photometer array after transformation into the polar coordinate system x*y* (θ*ϕ*) with $d_R = d_S = 650$ mm and $\theta_R = \theta_S = 15°$. Concentric circles are shown for θ* = 5°, 10°, 15°, 20°. Maximum inclination of light incidence is 24°, minimum inclination is 5° (covering about $\theta_S \pm 10°$).
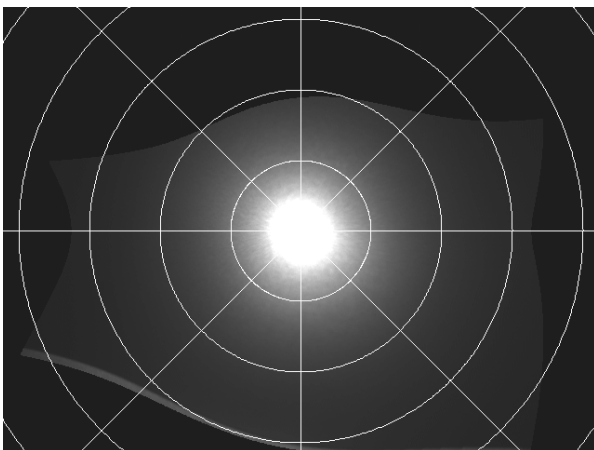

Figure 9: BRDF obtained by transformation of the PSF into the x*y*-coordinate system with circles for θ* = 5°, 10°, 15° and 20°. The brighter curved area in the background is the sample surface (computer monitor, over-exposed for illustration purposes).

In the next step, the intensities of the PSF as recorded with the imaging photometer (see for example fig. 1) are re-arranged and plotted into a polar coordinate system to obtain a representation as shown in fig.9.

4.2 Variation of sample illuminance

Depending on the light-source and its arrangement relative to the sample, different variations of illuminance across the surface of the sample are obtained.
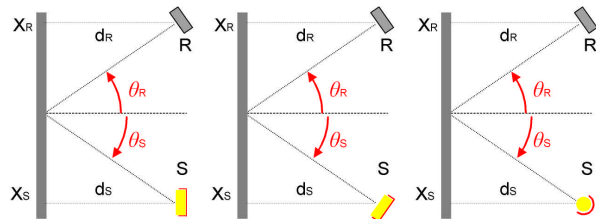

Figure 10: Illumination arrangements: flat Lambertian source parallel to the DUT-plane (left) and rotated by θ_S (center), isotropic source (right).

This variation of sample illuminance has to be carefully taken into account, since the BRDF is the quotient of the measured luminance divided by the illuminance at the corresponding location (see eqn. 5). Illuminance variations for the arrangements sketched in fig. 10 are proportional to $\cos^3\theta$ (for the isotropic source, right) and $\cos^4\theta$ (for the source parallel to the DUT-plane, left). The inclined flat source (center) represents an intermediate case.

4.3 Variation of photometer sensitivity

A further natural source of distortion of the measured luminance of the sample is the imaging photometer itself. In the simple case of a pinhole camera with its film-plane parallel to a plane object of uniform luminance the illuminance of the film is dropping proportional to $\cos^4\theta$ (θ being the angle between the optical axis of the camera and an oblique direction of light incidence) due to the shrinking of the solid angles related to the transfer of luminous flux. To avoid any distortion of the PSF luminance pattern by such effects, the variation of illuminance across the detector array is computed and the illumination corrected accordingly. Such a correction of the illuminance variation in imaging photometers is often called "flat-field correction" since a uniformly reflecting or emitting sample is expected to yield a uniform (flat) illuminance on the detector array.

A check for the model of sample illuminance and detector illuminance is performed with a Lambertian sample. When the modeling is correct, we obtain a uniform array of luminance values from the imaging photometer.

5 Measurement procedure

In the arrangement according to figure 2 both light source and imaging photometer are aligned with their optical axes in the plane perpendicular to the sample. This alignment is checked with a mirror in place of the DUT. The photometer is then focused to obtain a sharp image of the light source via the mirror and the position of the center of the light source is recorded. In the next step, the sample is introduced into the setup, replacing the mirror

and it is aligned in such a way that the center of the haze distribution is located as close as possible to the image of the light source. With these settings the luminance reflected by the sample is measured. We use multiple exposure times in order to extend the dynamical range of the photometer (controlled over-exposure), averaging of a multitude of individual exposures to improve the signal-to-noise-ratio of the measurement and corrections for the various dark-signals of the photometer.

A further measurement is required for evaluation of the illuminance across the DUT surface with a plane Lambertian reflector of known reflectance. The BRDF is then evaluated as the quotient of illuminance and luminance at each spot of the sample.
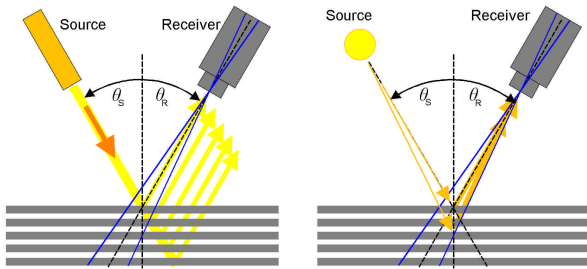

Figure 11: Illumination of a multilayer sample with a collimated beam (left) and with an isotropic point-source (right).

6   Evaluations

Typically we obtain three arrays of luminance values (2-dimensional distributions) from the measurement procedure as sketched above :

- luminance distribution of the light source (via a mirror),
- luminance distribution of the diffuse reflector (illuminance),
- luminance distribution of the DUT.

We have implemented software that transforms the luminance values numerically from the regular grid of the photometer into the polar coordinate system x*y* from the geometry data of the setup (e.g. angle of source and receiver inclination, θ_S, θ_R, d_R, d_S, x_R, x_S, etc.).

The maximum of the luminance reflected by the sample is chosen as the center of the x*y*-coordinate system. With all parameters defined and corrections performed the BRDF is finally computed as the quotient of sample illuminance and reflected luminance. Calibration of the BRDF can be achieved with calibrated diffuse reflectance standards and with calibrated non-scattering mirrors.

7   Results

Figure 9 shows the 2D-BRDF of the sample of fig. 4 (BRDF measured conoscopically) as obtained from the PSF. The contours of the region of transformation (originally a rectangular grid) is distorted in the same way as indicated in fig. 8. Figure 15 shows the IP-BRDF of the sample of fig. 4 obtained from the PSF at $\phi = 0°$ compared to the result obtained with a conoscopic method. The reduced resolution of the conoscopic approach is obvious by the different shapes of the curves, especially by the difference of the height of the specular peak.

Figure 16 presents different resolutions of the in-plane BRDF obtained from the PSF close to specular and illustrates how the

specular peak can be separated from the haze-hill by local fitting of parabolas to the high-resolution BRDF. A special 3-dimensional representation of the s ame data is shown in fig. 17.

Figure 18 is the IP-BRDF from the PSF of fig. 1 close to specular, showing interference effects of the beams reflected and diffracted by the pixel-pattern of the LCD-monitor.

8   Discussion

Compared to illumination with a collimated beam the point-source illumination schemes offer several advantages that are the basis of the inherent robustness of the method in various applications.

8.1   Point-source illumination

Application of a point source instead of a collimated beam source (CIE 38, 1977: max. deviation from the central ray is 5°) has some advantages with respect to the alignment of source, sample and receiver and for the measurement of multilayer samples [7].

In the case of a collimated beam illumination as shown in the right diagram of fig. 11, a multitude of mechanical degrees of freedom (max. 6) have to be controlled and adjusted to make sure that the light reflected in a specular way from e.g. the first surface arrives at the detector array of the receiver without unwanted attenuation.
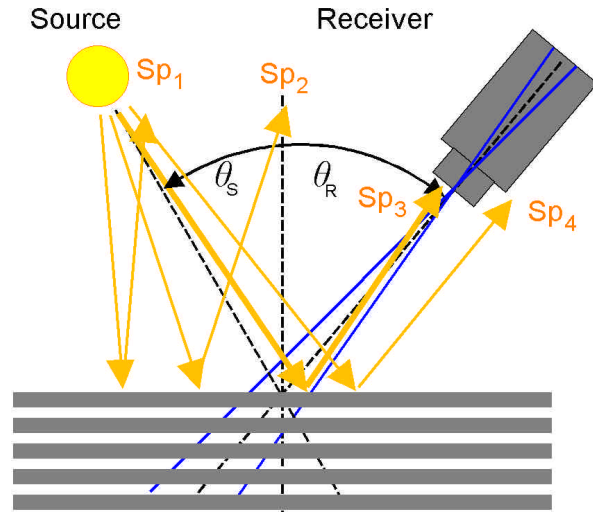

Figure 12: Specularly reflected beams $Sp_1...Sp_4$ from different locations on the sample surface. Sp_3 is received by the receiver with a non-specular inclination $\theta_R > \theta_S$.

The point-source illumination scheme is much more tolerant with respect to these alignments. If, for example, the inclination of the receiver should not be equal to the source inclination as shown in fig. 12, the receiver still captures one of the many specular beams, here Sp_3, however with an angle of inclination that is slightly different from θ_S. Also this beam, Sp_3, will not originate from the intersection of the optical axes of source and receiver on the sample surface as shown in fig. 12. When the geometry is chosen accordingly, especially when the distance of the source from the sample is sufficiently large, the variation of the inclinations of incident and received beam remain small for most practical purposes.

Another application demonstrating the advantages of the point-source illumination scheme is the evaluation of reflection components from multilayer stacks as illustrated in fig. 11 [7]. In the case of the collimated beam illumination the reflection components from the interfaces are separated and emerge as shifted parallel beams of which the receiver, depending on its aperture, can capture only a limited number. In the case of the point-source illumination, the partial reflection components can all be captured, but they have slightly different angles of inclination. The luminance image of an imaging photometer shows these reflection components as "pearls on a string", i.e. as a sequence of images of the source that are laterally displaced.

An argument against application of the point-source illumination scheme might be the non-uniformity of illuminance at the area-element actually measured (*field of measurement*) which is a function of the distance to the source, but this variation can be kept small enough when the source is sufficiently far away. Also, the problem of producing a collimated beam with high uniformity across the beam diameter it is often underestimated.

The most annoying side-effect of many real light-sources used as point sources is the non-uniformity of illuminance caused for example by the filament or the glass-bulb of incandescent lamps.

8.2 BRDF from PSF

The approach of deriving BRDF characteristics of LCD-screens from the PSF seems obvious to everyone who has been observing reflections of small light sources in display devices with bare eyes for a first qualitative judgement of the components of the BRDF. The general idea is mentioned e. g. in [8], but no details of the method and its implementation nor results have been presented and published so far.

The transformation from the PSF to the BRDF as introduced here maps the angles of inclination relative to the specular direction, and the azimuth-angles relative to the plane of specular and received beam, not taking into account their absolute values. This can be done as long as the BRDF is sufficiently constant with respect to variations of the direction of light incidence.

8.2.1 BRDF variations with angle of light incidence

In general, the BRDF of rough surfaces changes its shape with increasing angle of light incidence, becoming more skewed and asymmetrical [9]. We have analyzed the variation of the BRDF for two typical samples: an LCD-monitor and a scattering semi-gloss reference standard (made from etched black glass).

Figure 13 illustrates that the BRDF of the LCD-monitor keeps its basic shape, but the height of the specular peak varies with angle of light incidence as shown in fig. 14 (lower curve). It is also obvious that the width of the bell-shaped BRDF increases with angle of light incidence. We have also measured the height of the specular peak of a scattering semi-gloss standard for $\theta_S = 15°$, $30°$ and $45°$ as shown in fig. 14 (upper curve).

The shape of the BDRF-curve and the related variation of the height of the specular peak with angle of light incidence depends on both the material of the object and on the microtopography of its surface and is thus hard to predict without specific knowledge of the details [3].

The BRDF-variation with source inclination has also been analyzed in one specific case by E. F. Kelley, et al. [10]. Both peak value and shape remain fairly constant over a limited range of incident angles (e.g. $\theta_S = 3°$ to $30°$) with decreasing peak-height.
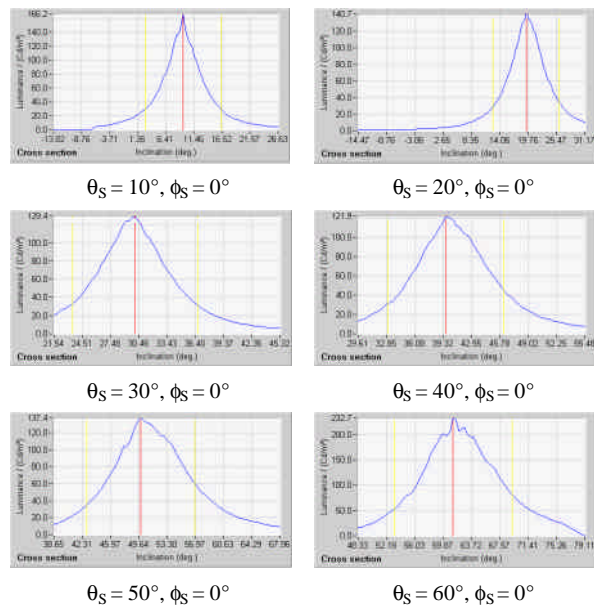

$\theta_S = 10°, \phi_S = 0°$ $\theta_S = 20°, \phi_S = 0°$

$\theta_S = 30°, \phi_S = 0°$ $\theta_S = 40°, \phi_S = 0°$

$\theta_S = 50°, \phi_S = 0°$ $\theta_S = 60°, \phi_S = 0°$

Figure 13: Variation of the BRDF of an LCD-monitor with angle of light incidence, θ_S. Conoscopic measurement, signature $\approx 1°$.
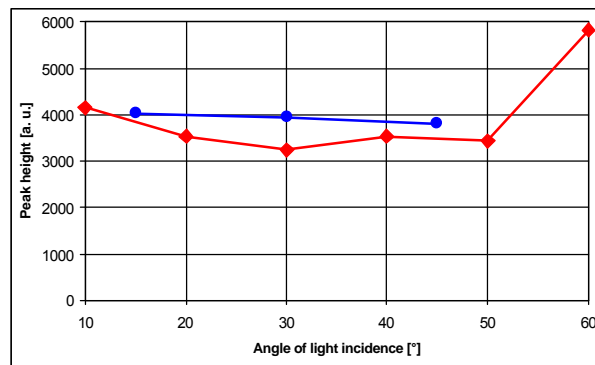

Figure 14: Variation of the peak height of the BRDF of the LCD-monitor of fig. 4 (lower curve) and of an etched scattering semi-gloss standard (upper curve) with angle of light incidence, θ_S.

The BDRF as obtained from the PSF as introduced here is exact at the specular direction. Variations with the angle of light incidence can easily be evaluated by variation of the inclination of the source, θ_S just as with other BRDF measurement methods (mechanical or optical scanning). It should also be noted that the range of angles of inclination in the typical PSF example of fig. 8 is restricted to $\theta_S \pm 10°$.

Visual observation of the PSF under various angles of light incidence confirms the impression of stability of the pattern of reflection (PSF). In this case however we must take into account that our eye perceives the PSF on a logarithmic scale. Further measurements are definitely required to analyze the variation of the PSF and the resulting BRDF of a variety of display related materials and layers with direction of light incidence.

8.2.2   BRDF variations over the sample surface

The reflective properties of the DUT must be sufficiently constant over the area included in the measurement. This requirement however has to be fulfilled anyway in the case of electronic displays.

8.2.3   More general aspects

The symmetry properties of the transformation can be used for widening the range of inclinations included in one measurement without loss of resolution (i.e. source-receiver signature).

After transformation of the PSF into the 2-dimensional BRDF the reflectance factors r_{S1} and r_{S15} according to Kubota (ISO 13406-2) can be obtained via the concept of the inverse-BRDF (application of the Helmholtz reciprocity). This means that while in the setup of Kubota the source aperture is varied, the same results can be obtained with a source with constant small aperture and a variable receiver aperture which is realized by integration over the BDRF.

The fact that the center of the reference coordinate system x*y* is aligned with the specular direction in the sample luminance distribution effectively minimizes errors caused by mechanical misalignments of the setup.

The introduced method is highly promising for precise and fast evaluation of a variety of appearance attributes (both in reflection and transmission), e.g. distinctness-of-image (DOI),clarity, haze, etc.. These characteristics can now be determined numerically from the PSF instead of doing this with pinholes and stops which are difficult to align mechanically with the required precision. The new method now allows centering of regions-of-interest in the PSF and BRDF corresponding to stops and apertures in the evaluation software, for example relative to the specular direction.

Recent experiments with directional (anisotropic) samples suggest that the method can as well be applied to that class of samples. Figure 1 actually shows the PSF of such a directional sample, with the anisotropy of reflection caused by diffraction of the regular structure of the LCD-pixels. Extension of the method to curved samples with arbitrary surface shapes is currently being done and will be published in a forthcoming paper.

The method is also well suited for spectral analysis of scattered light via the source and via the receiver.

9   Conclusions

The presented method extracts the BRDF of flat uniform samples from the PSF. The results, even though limited in their range of angles of inclination, feature a high angular resolution and can be used to accurately separate the specular peak from the haze. The method thus is extremely useful for fast evaluation of appearance attributes e.g. clarity, distinctness-of-image, haze, etc. with high resolution. Detailed evaluation of a variety of characteristics from the high-resolution BRDF and of the two reflectance factors needed for ergonomic rating of displays is thus made fast, easy and affordable.

References

[1] M. E. Becker: "Evaluation and Characterization of Display Reflectance", SID '97 Digest, pp. 827

[2] E. F. Kelley, G. R. Jones: "Utilizing the BRDF to predict reflections from FPDs", SID '97 Digest, pp. 831

[3] John C. Stover: "Optical Scattering, Measurement and Analysis", SPIE 1995

[4] S. Kubota: "Measurement of specular reflectance of LCDs", Proc. Int. Symp. Illum. Engin. Soc. Jpn., (1994), pp. 241

[5] M. E. Becker: "Measurement of Display Scattering", Proceedings of the 22nd IDRC 2002, pp. 803

[6] E. F. Kelley: "Sensitivity of Display Reflection Measurements to Apparatus Geometry", SID'02 Digest, pp. 140

[7] M. E. Becker: "Evaluation and Characterization of Display Reflectance", DISPLAYS 19 (1998), pp. 35

[8] E. F. Kelley: "FPD Measurements and Standards", SID Application Tutorials 2001, slide no. 79

[9] J. E. Harvey: "Modeling the image quality ...... as a surface power spectral density filter function", APPLIED OPTICS, 34, 19(2995), p. 3715-3726

[10] E. F. Kelley, et al. : "Display Reflectance Model Based on the BRDF", Displays, Vol. 19, No. 1, June 30, 1998, pp. 27-34 (June 1998) - BRDFs for 3°, 10°, 20° and 30°

10   Appendix - Derivation of ϕ* and θ*

With the incident beam, $\vec{SP}$, the specular beam, $\vec{SP^*}$, and the received beam, $\vec{PR}$, as functions of the geometry parameters according to fig. 2

$$\vec{SP} = \begin{bmatrix} x - x_S \\ y \\ -d_S \end{bmatrix}, \ \vec{PS^*} = \begin{bmatrix} x - x_S \\ y \\ d_S \end{bmatrix}, \ \vec{PR} = \begin{bmatrix} x_R - x \\ -y \\ d_R \end{bmatrix} \quad A1$$

the plane containing both the specular and the received beam is given by:

$$\vec{r} = \gamma \cdot \vec{PR} + \delta \cdot \vec{PS^*}. \quad A2$$

The line of intersection of this plane with the x*y*-plane of the inclined coordinate system x*y*z* is given by:

$$\alpha \cdot \vec{x^*} + \beta \cdot \vec{y^*} = \gamma \cdot \vec{PR} + \delta \cdot \vec{PS^*}. \quad A3$$

From that we obtain the azimuth ϕ* as follows:

$$\phi^* = \arctan\left(\frac{A \cdot y + B \cdot (x_S - x)}{A \cdot (x - x_S) + B \cdot y} \right), \quad A4$$

with

$$A = \frac{(x - x_S) \cdot (x_R - x) - y^2 - \frac{d_R}{d_S}\left((x - x_S)^2 + y^2\right)}{(x - x_S)^2 + y^2 + \left(\frac{(x - x_S)^2 + y^2}{d_S}\right)^2}, \quad A7$$

and

$$B = \frac{y \cdot (x_R - x)}{y^2 + (x - x_S)^2}. \quad A8$$

The angle of inclination of the received beam with respect to the specular beam becomes

$$\theta^* = \arccos\left(\frac{(x - x_S) \cdot (x_R - x) - y^2 + d_S \cdot d_R}{\sqrt{(x - x_S)^2 + y^2 + d_S^2} \cdot \sqrt{(x_R - x)^2 + y^2 + d_R^2}} \right). \ A9$$
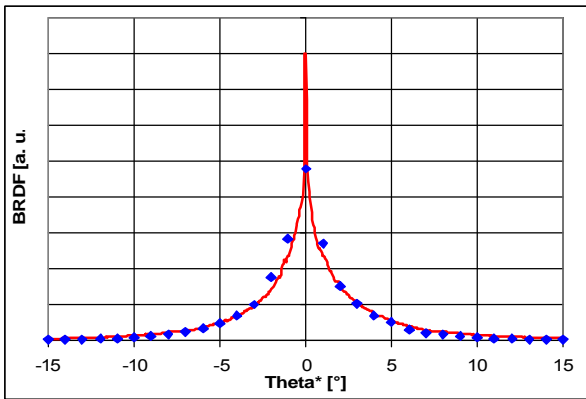
Michael E. Becker

Figure 15: Comparison of IP-BRDF-curves obtained from the PSF (solid curve) and obtained with a conoscopic approach (diamonds, compare fig.4). The difference of the curves is caused by the different source-receiver signatures which are FWHM $\approx 1°$ in the conoscopic measurement and FWHM $\approx 0.2°$ for the new PSF-method. Note, that there is a significant difference in the height of the peaks at the specular direction.
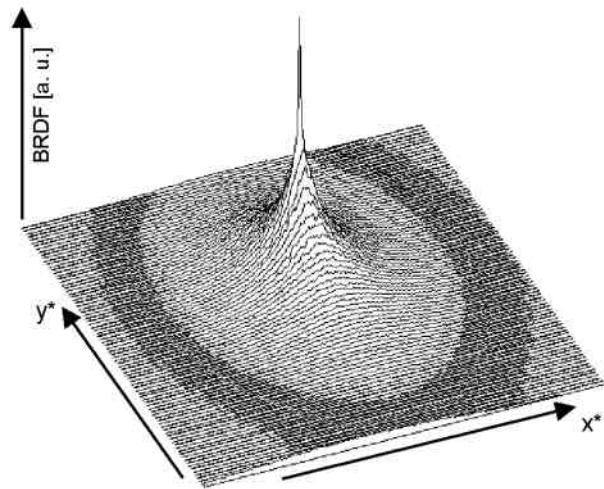

Figure 17: 2-dimensional BRDF of the LCD-screen of fig. 4, fig. 15 and 16. shown as a 3-dimensional surface plot in the x*y*-coordinate system for better visualization of the decrease of the haze with distance from the peak at the specular direction.
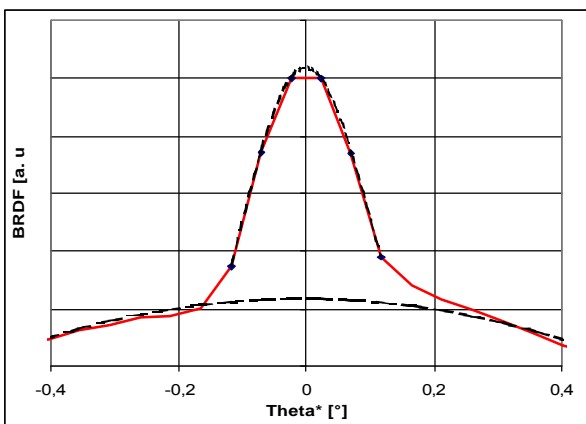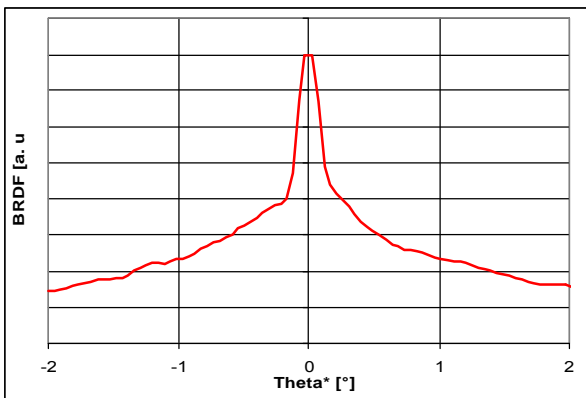

Figure 16: IP-BRDF from the PSF of the sample of fig. 4 close to specular, $\theta_S = 15°$. Local fitting of two parabolas for separation of the specular peak from the haze hill (bottom).
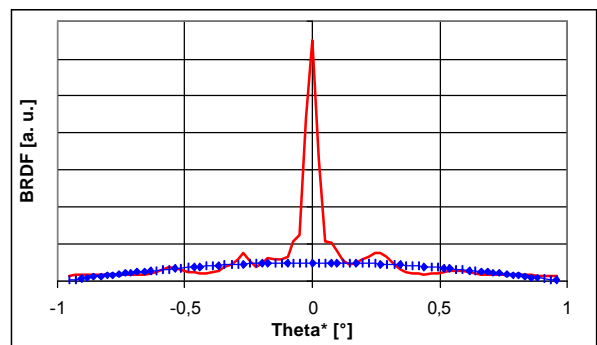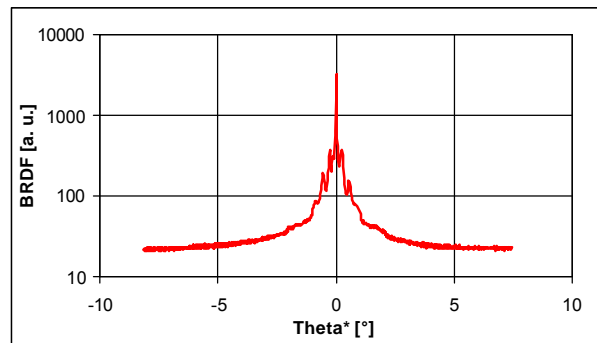

Figure 18: IP-BRDF from the PSF of the sample of fig. 1 with diffraction and interference effects. Local fitting of a parabola for separation of specular peak from haze hill (bottom). Since the spatial frequency of the pixel-pattern of the LCD is higher in the horizontal direction than in the vertical, the intensity modulation caused by diffraction and interference is more pronounced in the horizontal direction (see figure 1).